Proc. Indian Acad. Sci. (Chem. Sci.), Vol. 95, Nos 1 & 2, July 1985, pp. 59–75.

NMR imaging: Mathematical modelling and spectrometer design considerations

P RAGHUNATHAN,* S KRISHNAN‡ and K R SRIVATHSAN‡

Departments of *Chemistry and ‡Electrical Engineering, Indian Institute of Technology, Kanpur 208 016, India

Abstract. The mathematical modelling of 'NMR imaging' is presented from the electrical system design viewpoint. The response, namely, the magnetisation $M_{xy}(t)$, is linearly related to a system identification function made up of the nuclear spin density distribution $\rho(\mathbf{r})$ and the relaxation times $T_1(\mathbf{r})$ and $T_2(\mathbf{r})$, while the r.f. excitation affects the system nonlinearly and appears as an 'aperture' function in the imaging equation.

Spectrometer design considerations indicate that the resolution is limited by noise at the detection stage. In our imaging spectrometer developed for studying multiphase biospecimens, a 1 mm image resolution is feasible with a gradient of 50 $\mu T\,cm^{-1}$, assuming a 200 Hz frequency resolution and signal averaging.

Keywords. NMR imaging; mathematical modelling; NMR imaging spectrometer; Zeugmatography.

1. Introduction

The use of nuclear magnetic resonance (NMR) as an important imaging technique originated with Lauterbur (1973) who proposed the addition of linear field gradients to the homogeneous magnetic field in order to transform the conventional (*i.e.*, zero-dimensional) NMR signals into projections which represent integrated values of the signals along lines or planes of an object. NMR imaging, or *zeugmatography* as Lauterbur originally called it, is thus already a decade old, and the initial experiments have stimulated the evolution of various modalities within the main framework of NMR.

However, with the present-day requirements of full-scale systems for use in a variety of biophysical and biomedical applications, it becomes necessary to identify, if not indeed unify, the common elements underlying the various modalities. Any meaningful comparison of several possible approaches to NMR imaging, from the electrical 'systems' viewpoint, necessitates the development of appropriate imaging equations based on a mathematical model. For the conventional NMR phenomenon, a good mathematical model is already available in the form of the well-known Bloch equations (Bloch 1946). However, the nonlinear characteristics of a 'driven' NMR system have somewhat restricted the development of simple quantitative models for describing the response, especially to arbitrary excitation pulses. This important point has been made recently in several elegant descriptions of NMR imaging (Hoult 1979; Mansfield *et al* 1979; Caprihan 1983; Hinshaw and Lent 1983).

Before discussing the mathematical model, we briefly recall the basic theory of NMR and NMR imaging, and review the presently known imaging modalities in the following

* To whom all correspondence should be addressed.

three sections. In § 1.4, an overview is given of the essential radiofrequency (r.f.) pulse sequences and magnetic field gradients which provide the input 'excitations' to the nuclear spin system.

In § 2 we develop the mathematical model based on the 'systems' approach, and critically examine the imaging equations from several points of view. In § 3 are derived the response functions when the system is driven by basic excitations characteristic of several imaging modalities. In § 4, reception of the response signal is considered, and 'noise' and the spectrometer 'figure of merit' are discussed. Lastly, we outline the design criteria adopted in the construction of an imaging spectrometer in our chemistry laboratory for studying multiphase biosamples, and present its block schematic diagram.

1.1 *Some basic theory*

A nucleus with an odd mass number such as ^{1}H possesses the quantum mechanical property of intrinsic *spin* angular momentum. $\mathbf{I}\hbar$, the possession of both spin and charge conferring on it a magnetic dipole moment $\mu = \gamma\hbar\mathbf{I}$ (recall the classical electromagnetic analogue of a charged mass spinning in a circular orbit generating a magnetic moment). According to fundamental NMR theory (Abragam 1961), when a physical specimen containing an ensemble of such dipoles is polarised in a constant d.c. magnetic field $\mathbf{B}_0$ along, say, the z-direction of the xyz laboratory coordinate system, it develops a macroscopic magnetisation, $\mathbf{M}$, which is the vector sum of the μ's of the individual nuclei. $\mathbf{M}$ then experiences a torque proportional to $\mathbf{M} \times \mathbf{B}_0$ at the angular rate

$$\omega = -\gamma\mathbf{B}_0 \tag{1}$$

and the differential equation governing this precessional motion is given by

$$\mathrm{d}\mathbf{M}/\mathrm{d}t = \gamma\mathbf{M} \times \mathbf{B}_0. \tag{2}$$

The introduction of a circularly polarised r.f. magnetic field $\mathbf{B}_1(t)$ (at the angular frequency ω) in the plane orthogonal to the z-axis tends to 'nutate' the magnetisation $\mathbf{M}$ about its instantaneous axis, and 'resonant absorption' of r.f. energy occurs. In the xyz frame, the nett magnetisation is now the resultant $\mathbf{B}_{res} = \mathbf{B}_0 + \mathbf{B}_1(t)$, and the resultant nutation frequency is $\omega_{res} = -\gamma\mathbf{B}_{res}$.

Mathematically, resonance is better handled by adopting a reference frame $x'y'z'$ which *rotates* about the z-axis at frequency ω in the same sense as the precessing nuclear magnet. The effect of $\mathbf{B}_0$ gets subsumed in this rotating frame, and we have

$$|\omega_{res}|_r = \gamma|\mathbf{B}_1|_{max}. \tag{3}$$

$(\omega_{res})_r$ is the nutation frequency in the rotating frame, and is an important variable in NMR.

If the r.f. field is left on for a duration t_p, the angle ϕ by which $\mathbf{M}$ nutates is given by

$$\phi = \gamma|\mathbf{B}_1(t)|\,t_p. \tag{4}$$

ϕ is termed the nutation of 'flip' angle. Remembering in our formulation that the observation plane for the magnetisation is $x'y'$, it is seen that to obtain maximum NMR signal response due to the nett transverse component $\mathbf{M}_{x'y'}$, ϕ must be 90°. The application of a $\pi/2$- or 90°-r.f. 'pulsed' excitation achieves this. As a further important part of NMR terminology, we mention here that, subsequent to the 90° r.f. pulse the decay

of the $\mathbf{M}_{x'y'}$ response signal in the time domain, $s(t)$, is called the *free induction decay* (FID).

The basic mathematical model of NMR is developed from the differential equation of motion, equation (2), in the rotating frame, and includes the two important relaxation times, T_1 and T_2. The first of these, the spin-lattice relaxation time, characterises the restoration of thermal equilibrium of the spin ensemble with the 'lattice', or return of the nett magnetisation to the z-axis in presence of $\mathbf{B}_0$. On the other hand, T_2 is characteristic of the loss of phase information amongst the spins under the influence of the 'spread' in the local dipolar field, and does not lead to restoration of thermal equilibrium of the overall spin-lattice system. Addition of these two rate factors to (2) completes the set of Bloch phenomenological equations,

$$\frac{\mathrm{d}\mathbf{M}_{x'y'}}{\mathrm{d}t} = \gamma \mathbf{M} \times \mathbf{B} - \frac{M_x}{T_2}\mathbf{i}_x - \frac{M_y}{T_2}\mathbf{i}_y - \frac{(M_0 - M_z)}{T_1}\mathbf{i}_z. \tag{5}$$

In (5), $\mathbf{B} = B_0\mathbf{i}_z + B_{1x}(t)\mathbf{i}_x + B_{1y}(t)\mathbf{i}_y$ is the resultant magnetic field ($\mathbf{i}_x$, $\mathbf{i}_y$ and $\mathbf{i}_z$ being unit vectors), and B_{1x} and B_{1y} are the components of the circularly polarised r.f. magnetic field. In the terminology of electrical signal systems, the Bloch equations thus typify a 'lumped' model wherein the vector dynamical equation of the bulk nuclear magnetisation is established taking account of the damping factors due to the two spin relaxation mechanisms.

1.2 *Principles of NMR imaging*

The concept of 'imaging' an object using NMR follows logically from the background in the previous section. The resonance equation (1), implies that the superposition of a spatially varying magnetic field $\mathbf{B}(r)$ over $\mathbf{B}_0$ amounts to a spatial variation of the resonance frequency

$$\omega(\mathbf{r}) = -\gamma(\mathbf{B}_0 + \mathbf{B}(r)). \tag{6}$$

The variation $\omega(\mathbf{r})$ is linear if $\mathbf{B}(\mathbf{r})$ varies linearly over $\mathbf{r}$. $\mathbf{B}(\mathbf{r})$ may be written as

$$\mathbf{B}(\mathbf{r}) = -\mathbf{G}(\mathbf{r})\cdot\mathbf{r}, \tag{7}$$

where $\mathbf{G}(\mathbf{r})$ is the magnetic field gradient. In the simple case of a field gradient in the x-direction,

$$\omega(x) = -\gamma(\mathbf{B}_0 + \mathbf{G}_x \cdot x), \tag{8}$$

where the gradient is imposed over the main magnetic field.

Alternatively, (8) implies a mapping between the spatial coordinate x and the frequency $\omega(x)$. The primary response in NMR imaging is the distribution of the *density* of nuclear spins, say, the protons. In a proton-containing object, this amounts to an image-formation, with the spin density distribution denoting the intensity of the image. One should also note that the resolution is determined by the magnitude of the magnetic field gradient $G_x(x)$ rather than the wavelength of excitation.

1.3 *A review of current imaging modalities*

NMR imaging is marked by a variety of ways of obtaining a map of the nuclear density distribution in an object. The reason for this is the basic imaging equation itself, as will transpire in the next section. Heuristically, the argument is based on the fact that the

field gradient, in conjunction with the r.f. excitation, is capable of confining the NMR response to a small region in space. Therefore, the various modalities represent the ways in which the sample responses may be grouped together for spatial encoding.

Broadly, imaging modalities may be classified as being 'reconstructive' or 'non-reconstructive'. The former technique is an adaptation of the principles of image generation in x-ray computerised tomography (Hounsfield *et al* 1973; Scudder 1978), and involves reconstruction of the image in its entirety from integral projections. The procedure for extracting the image from a signal received in the time domain, $s(t)$, may be understood from

$$s(t) = \int_x \rho(x) \exp(i\gamma G_x x t)\, dx, \tag{9}$$

which indicates a Fourier transformation between $\rho(x)$ and $s(t)$, where

$$\rho(x) = \int_y \int_z \rho(xyz)\, dy\, dz. \tag{10}$$

Thus $s(t)$ contains the *plane integral*, equation (9). The image is then obtained by invoking a suitable algorithm for 'back-projecting' (see figure 1) to reconstruct a 3-D or 2-D image from projections. This necessitates scanning the object space, which is also the $K_x - K_y$ phase space ($K_x = \gamma G_x \cdot x$, $K_y = \gamma G_y \cdot y$; see the phase factor in (9)) probed by the magnetic field gradients (Locher 1984).

Modalities in which an image reconstruction scheme is not involved are classified as non-reconstructive. Successful techniques that fall under this classification are (i) the point and line-scan imaging (Mansfield and Maudsley 1976; Maudsley 1980), (ii) direct Fourier transform (DFT) imaging (Kumar *et al* 1975), and (iii) sensitive-point imaging

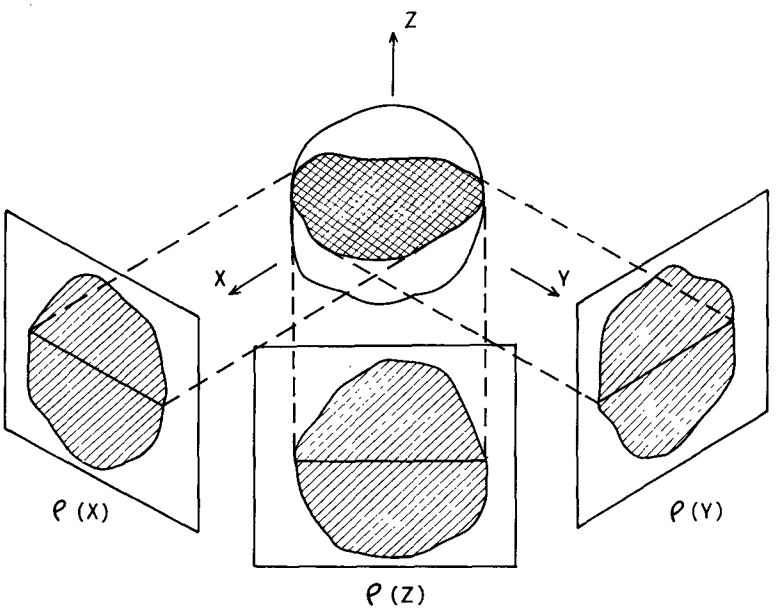

Figure 1. A pictorial representation of 'reconstruction', where the plane integrals are back-projected to obtain the image.

(Hinshaw 1976). Point and line-scan imaging may be accomplished by selectively 'exciting', or bringing into resonance, a particular region of the sample (a line or a point) at a time, and recording the response. The process is repeated to map the whole sample region. A detailed discussion of this modality has been published recently (Cho *et al* 1982).

DFT imaging involves line-scanning the phase plane, so that spatial information is encoded into the *phase* behaviour of the spin magnetisation. The data is processed either in 2-D or 3-D format depending on the mode of scanning which is achieved by switching the x, y and z-gradients, and is then subject to a direct Fourier transform for image formation. Often this is *the* preferred modality of imaging in biomedical contexts.

The third modality, sensitive-point imaging, uses time-dependent magnetic field gradients for recovering spatially resolved signals. The field gradient is carefully set up to be time-dependent everywhere except within a small region of interest, the 'sensitive point'. Because the NMR signals from the regions of time-dependent field are frequency-modulated, only the sensitive point gives a nonvanishing signal after low-pass filtering. Then, by controlled variations of the relative currents in the coils supplying the alternating gradients, the sensitive 'spot' may be shifted in much the same way as the scanning spot in TV, to build up a complete scan (or 'raster') in, say, the xz plane, thus producing an image 'slice' through the object. A stack of such slices provides the complete 3-D image. Data acquisition here is slow, and affects imaging time—an important factor in biomedical applications.

1.4 *Modes of excitation of the system being imaged*

1.4a *R.f. pulses*: The $\mathbf{B}_1$-field may be tailored to stimulate either the whole sample or specific regions. Consequently, there are (a) 90° and 180° broadband pulses and (b) 90° and 180° narrow-band pulses. The power spectra of the broadband pulses are designed to excite the whole sample in the presence of strong field gradients. The power requirements on these pulses are, however, large; they are therefore sparingly used in imaging experiments. In most imaging techniques, 90° pulses initiate a sequence and may be applied before imposing the field gradients, thereby obviating the necessity for broadband stimulus.

The narrow-band 90° and 180° r.f. pulse excitations are used to stimulate selectively a region of the sample, and are important in non-reconstructive modalities, *e.g.* to effect slice selections in 2-D DFT imaging.

1.4b *Magnetic field gradients*: The two types of field gradients used in imaging are (a) read-out gradient and (b) pulsed gradient. The first is a constant gradient applied in a particular direction, say the x-axis, for a duration t much longer than the spin-dephasing time, $t \gg 1/\gamma G_x L$ (where L is the spatial extent of the sample over which FID signals are collected). The purpose is to effect the read-out of the response, and is used in line-scan and DFT imaging.

The term 'pulsed gradient' refers to the case where the duration of the gradient is shorter than the spin dephasing time so that the transverse magnetisation remains in phase, while being modified marginally by the pulse.

2. Mathematical model of NMR imaging: A 'systems' approach

The characteristics of NMR imaging for purposes of 'system identification' depend on the three most important parameters, $\rho(\mathbf{r})$, $T_1(\mathbf{r})$ and $T_2(\mathbf{r})$. Mapping the spatial information onto the frequency spectrum is achieved by applying $\mathbf{G}(\mathbf{r})$. Consequently, considering the total NMR system as a black box, the inputs are $\mathbf{G}(\mathbf{r})$ and the r.f. excitation, $\mathbf{B}_1(t)$, while the output is the FID, $s(t)$. The main magnetic field B_0 defines the operating frequency of the experiment and is not presented as an input, since some form of demodulation or frequency translation is inherently assumed. Figure 2 describes schematically our 'systems' approach. The following remarks may be made at the outset before commencing our analysis: (a) the relationship between the input and output is involved, due to the nonlinearity of the Bloch equations; (b) the system is 'multi-input' and 'single-output' in nature, a fact to be borne out by the model to be developed, and (c) any linearity in the system, if present, is not obvious on a cursory examination.

In the rotating reference frame $x'y'z'$, we define (a) the residual field due to the field gradient at location $\mathbf{r}$ as $\Delta B(\mathbf{r})$, and (b) the frequency of $\mathbf{B}_1(t)$ as ω_0. The Bloch equation in the rotating frame is then modified to

$$(\mathrm{d}M/\mathrm{d}t)_{\mathrm{rot}} = (\mathbf{M})_{\mathrm{rot}} \times \mathbf{B}^* - \frac{M_{x'}}{T_2}\mathbf{i}_{x'} - \frac{M_{y'}}{T_2}\mathbf{i}_{y'} - \frac{(M_{z'} - M_0)}{T_1}\mathbf{i}_{z'}, \tag{11}$$

where $\mathbf{B}^* = \Delta B(r)\mathbf{i}_{z'} + B_1(t)\mathbf{i}_{x'} + 0.\mathbf{i}_{y'}$ (obtained by choosing the x-axis along the $B_1(t)$ phasor) and, by definition, $(\mathbf{M})_{\mathrm{rot}} = M_{x'}\mathbf{i}_{x'} + M_{y'}\mathbf{i}_{y'} + M_{z'}\mathbf{i}_{z'}$, all components being functions of t and $\mathbf{r}$ (with respect to the laboratory frame). Since orthogonal components of the magnetisation in the transverse plane of the rotating coordinates have a quadrature phase relationship in the laboratory frame, we define M as $M = M_{x'} - iM_{y'}$ and simplify the Bloch equations as

$$\frac{\mathrm{d}M}{\mathrm{d}t} + \left(\frac{1}{T_2} - i\gamma\Delta B(\mathbf{r})\right)M = -i\gamma\mathbf{B}_1(t)M_{z'},$$

$$\frac{\mathrm{d}M_{z'}}{\mathrm{d}t} = \gamma\mathbf{B}_1(t)\,\mathrm{Im}\,(M) - \frac{M_{z'} - M_0}{T_1}. \tag{12}$$

The term corresponding to T_1 may be neglected for all $t < T_1$. We have written the Bloch equations for a spatial location $\mathbf{r}$ in the sample, so that $M_{x'}$, $M_{y'}$, $M_{z'}$, T_1 and T_2 are functions of $\mathbf{r}$ (the location in the laboratory frame).

The NMR response is observed in the $x'y'$ plane, and so $M(t)$ is the variable of interest. The vector dynamical equations are then coupled, and nonlinearity is imposed through the time-varying r.f. field envelope $\mathbf{B}_1(t)$ which appears as a coefficient in the differential equations above. When $\mathbf{B}_1(t) = 0$, a situation that prevails at the end of the r.f. pulse, the evaluation of M is governed by linear differential equations. Therefore the FID signal

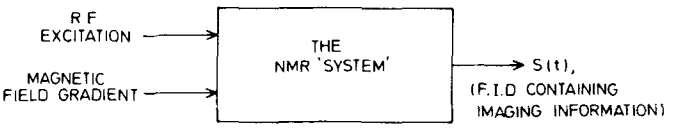

Figure 2. 'Systems' approach to NMR imaging.

may be regarded as the output of a linear system whose initial conditions are related to $B_1(t)$ in a nonlinear fashion. This important point emerges more clearly from our geometrical arguments that follow.

2.1 *The basic NMR imaging equation (from geometrical arguments in the rotating reference frame)*

We shall now construct the imaging equation by considering purely geometrical aspects of the precessing magnetisation. We assume that the resonance condition, equation (1), holds for the pulse duration t_p, and that $t_p \ll T_1, T_2$. We further assume that the modulating r.f. pulse envelope is rectangular, *i.e.*, $B_1(t) = B_1$, a constant, for $0 \leqslant t \leqslant t_p$. For simplicity we consider a single gradient $\mathbf{G}_x$ along the x-direction. The symbols to be used in our treatment are (i) $M_0(x)$, the equilibrium magnetisation in the interval Δx around x; (ii) $\rho(x)$, the one-dimensional spin density distribution, equation (10), and (iii) A, the cross-sectional area of the sample.

Figure 3 illustrates the precession of the resultant magnetisation in the $x'y'z'$ frame. The precession cone, indicated by broken lines in the figure, has its axis tilted by θ with respect to the z' axis. The cone degenerates to a circle at $x = 0$ where $\Delta\mathbf{B}(x) = 0$. The associated equations are $|\mathbf{B}_{res}| = [(\Delta\mathbf{B})^2 + \mathbf{B}_1^2]^{1/2}$, $\tan\theta = B_1/\Delta B = B_1/G_x x$ where θ is the 'tilt' angle, and $\phi = \gamma|\mathbf{B}_{res}|t_p$ is the 'flip' angle.

At time t_p, the magnetisation has the orientation determined by ϕ, θ and $M_0(x)$. For a general initial condition $\phi_1 = \phi|_{t=0}$ ($\neq 0$), the projections of the magnetisation along the x', y' and z' axes are

$$\begin{aligned} M_{x'} &= M_0(x)\{\cos\psi \sin\theta - \sin\psi \cos(\phi_1 + \phi_r)\cos\theta\}, \\ M_{y'} &= M_0(x)\{\sin\psi \sin(\phi_1 + \phi_r)\}, \\ M_{z'} &= M_0(x)\{\sin\psi \cos(\phi_1 + \phi_r)\sin\theta + \cos\psi \cos\theta\}, \end{aligned} \tag{13}$$

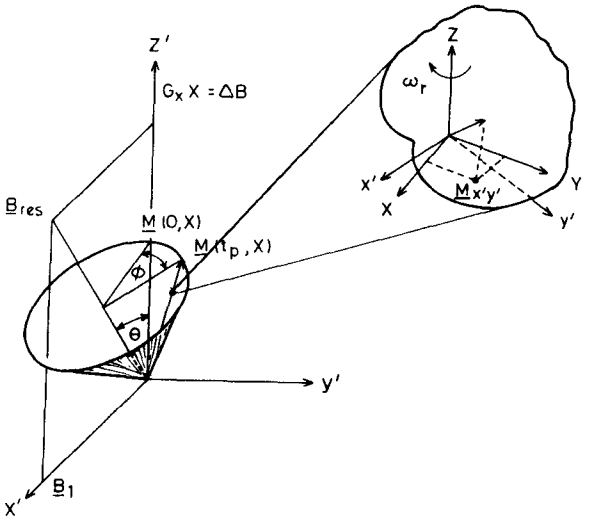

Figure 3. Precession of nuclear spin magnetisation in the rotating frame. The precession cone has its axis tilted away from z' by θ. Exploded inset shows the projection of the instantaneous magnetisation, $M(t_p, x)$, onto the $x'y'$ plane.

where ψ is the semiconical angle (or the angle between the vectors $\mathbf{B}_{res}$ and $\mathbf{M}(r, t)$), and ϕ_r is the instantaneous flip angle.

At the end of the r.f. pulse, the magnetisation precesses freely about the z-axis at a rate $\Delta\omega = \gamma \Delta B_x$, and therefore,

$$M_{x'}(x) = M_0(x) F_{x'}(x),$$

and

$$M_{y'}(x) = M_0(x) F_{y'}(x),$$

where $F_{x'}$ and $F_{y'}$ are the projections, or *aperture functions*, of $M_0(x)$ at time t_p. Writing $M(x)$ as

$$M(x) = M_{x'}(x) - iM_{y'}(x),$$

or

$$F(x) = F_{x'}(x) - iF_{y'}(x) = \frac{1}{M_0(x)}(M_{x'} - iM_{y'}), \tag{14}$$

the magnetisation $M_0(x)$ in turn may be expressed as

$$M_0(x) = K\rho(x),$$

where K is a constant of proportionality relating nuclear spin density to magnetisation. At the end of the pulse duration, $M_{x'y'}(x) = KF_{x'y'}(x)\rho(x)$, where the subscripts indicate that the phasors M and F are in the $x'y'$ plane, and are implicitly assumed henceforth. The future evolution of the magnetisation is determined by the field gradient $\Delta B = G_x x$. Thus,

$$M(t) = KF(x)\rho(x)\exp(i\gamma G_x x t).$$

The overall response from the entire sample aggregate is the magnetisation $m(t)$, where

$$m(t) = KA \int_x F(x)\rho(x) \exp(i\gamma G_x x t)\, dx. \tag{15}$$

So far in our derivation the effect of T_1 and T_2 has been neglected on the assumption that $t_p \ll T_1, T_2$ which is not valid for the long-term evolution of the magnetisation. Their first order effect (when $1/G_x L \ll T_2$) is a multiplicative term, $\exp(-t/T_2) f(T_1)$, and hence

$$m(t) = KA\left[\int_x F(x)\rho(x)\exp(i\gamma G_x x t)\, dx\right] \exp(-t/T_2) f(T_1). \tag{16}$$

This expression, cast in the form of a Fourier transformation, is the basic imaging equation. The term $F(x)$ is the aperture function modifying the effect of $\rho(x)$.

For the most common case of a rectangular pulse, applied to bring about a 90° flip of the magnetisation, $\phi_1 = 0$ and $\psi = \theta$ in (13), combining these with (14), one gets

$$F(x) = \sin\theta \cos\theta (1 - \cos\phi) - i \sin\theta \sin\phi, \tag{17}$$

while the expression is fairly complex in the case of arbitrary pulse excitations. The imaging equation, (16), leads to the following important observations:

(i) the response $m(t)$ is linearly related to the system identification parameter, $\rho(x)$;
(ii) the aperture function, $F(x)$, is nonlinearly related to the r.f. excitation, $B_1(t)$.

Equation (16) assumes an even more general form when the relaxation effects are spatially-dependent, and are therefore no longer exponential. The resultant transverse magnetisation (*i.e.*, signal) in 3-D would then be represented as

$$m(t) = K \int_V F(\mathbf{r})\rho(\mathbf{r})L(\mathbf{r}, t)\exp(i\gamma[\mathbf{G}(r)\cdot\mathbf{r}]t)\,\mathrm{d}V. \tag{18}$$

Our master equation, (18), may be interpreted in terms of *transfer functions*, where $\rho(\mathbf{r})$ and $L(\mathbf{r}, t)$ define the system parameters to be identified, and $m(t)$ may be treated as the impulse response of the transfer function $F(\mathbf{r})\rho(\mathbf{r})L(\mathbf{r}, t)$ as shown in figure 4.

2.2 *Arbitrary excitations: Use of perturbation techniques*

For the usual case of rectangular r.f. pulses, and for $\mathbf{B}_1 \cong G_x x$, it is easily seen from (17) that the components of $F(x)$ in the observation plane are

$$F_{x'}(x) = \frac{B_1|G_x x|}{[B_1^2 + (G_x x)^2]^{1/2}}\{1 - \cos(\gamma[B_1^2 + (G_x x)^2]^{1/2} t_p)\},$$

and

$$F_{y'}(x) = B_1 \gamma t_p \,\mathrm{sinc}(\gamma[B_1^2 + (G_x x)^2]^{1/2} t_p). \tag{19}$$

The solution for arbitrary excitations, however, may be obtained numerically using a piecewise rectangular approximation in the rotating frame (Caprihan 1983). Indeed, it may be shown that Gaussian, sinc and triangular modulations are 'good', if not optimum, r.f. excitations. More generally, the application of perturbation expansion techniques (Hoult 1979; Raghunathan 1981) helps one either to determine $F(x)$ or to design the $B_1(t)$ pulse to obtain a specific form for $F(x)$. This procedure may be important in selective excitations where image resolution is mainly determined by the aperture function.

In the perturbation approach, the magnetisations $M(t)$ and $M_{z'}(t)$ are written as a series of terms of order $\gamma B_1(t)$,

$$M(t) = M^{(0)} + M^{(1)} + \ldots,$$

$$M_{z'}(t) = M_{z'}^{(0)} + M_{z'}^{(1)} + \ldots. \tag{20}$$

For the general perturbation terms $M^{(n)}$ and $M_{z'}^{(n)}$, the Bloch equations yield (Hoult 1979)

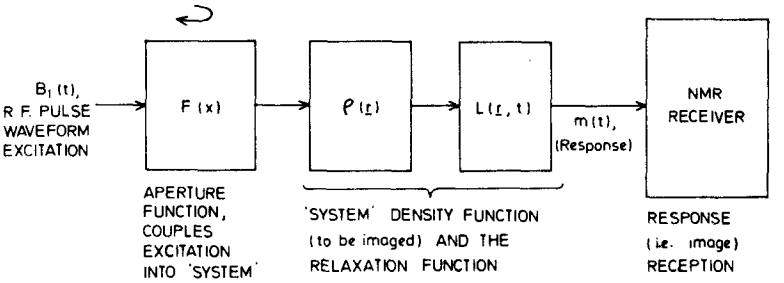

Figure 4. Excitation ($\mathbf{B}_1(t)$), Transfer ($F(x)\rho(\mathbf{r})L(\mathbf{r}, t)$) and Response ($m(t)$) functions involved in NMR imaging. The curved arrow signifies that the 'aperture' $F(x)$ is nonlinearly related to the r.f. excitation.

$$\frac{dM^{(n)}}{dt} + \left(\frac{1}{T_2} - i\gamma\Delta B(\mathbf{r})\right)M^{(n)} = -i\gamma B_1(t)M_{z'}^{(n-1)},$$

$$\frac{dM_{z'}^{(n)}}{dt} = \gamma B_1(t)\,\mathrm{Im}\,M^{(n-1)}, \tag{21}$$

with the initial conditions $M^{(0)} = 0$ and $M_{z'}^{(0)} = M_0(\mathbf{r})$, while the effect of T_1 is neglected.

The above equations are recursive; the equations for the first few orders lead to the results,

$$M_{z'}^{(1)} = 0,\ M^{(2)} = 0,\ M_{z'}^{(2)} = \int_{-\infty}^{t} \gamma B_1(t)\,\mathrm{Im}\,M^{(1)}t\,dt. \tag{22}$$

The following interesting result transpires from the above. At $\mathbf{r}_0$, where $\Delta B(\mathbf{r}_0) = 0$, M_0 precesses about $B_1(t)$ or the x' axis. The flip angle for this case is given by $\phi = \gamma|B_1|t_p$. Since the effect of the perturbation term is in the product $|B_1|t_p$ (or in B_1 for a given t_p), the flip angle may be treated as an indicator of the nonlinearity.

Some other important observations resulting from the perturbation solutions of the Bloch equation are: (i) the equation governing $M^{(1)}$ is linear, and predominant, for small flip angles, and operation in the linear region has the advantage of easy system design as $F(x) = \mathcal{F}(B_1(t))$, $\mathcal{F}$ denoting Fourier transformation; (ii) in the presence of a strong, linear field gradient, the magnetisation $M^{(1)}$ at time t_p is negligible, and may be observed only with a 'spin echo' pulse sequence (Hahn 1950; Carr and Purcell 1954); this is due, of course, to quick spin-dephasing by the gradients; (iii) the r.f. excitation should not possess sharp edges, as this increases side-lobe power in the primary response which reduces selectivity.

The Bloch equations and our geometrical arguments presented in the previous section are related by the fact that, while the former reflect magnetisation dynamics in the $x'y'z'$ frame, we treat the problem in a frame somewhat tilted with respect to the $x'y'z'$ axis system. The vector $\mathbf{B}_{res}$ (figure 3) is along one of the axes of this tilted frame. It may be derived from our geometrical formulation that, for $\Delta B < (B_1)_{max}$, $M_{y'} = -iM_0(x)\sin\phi$. The perturbation term $M^{(n)}$ of (21) corresponding to this situation then takes the form (Raghunathan 1981)

$$M^{(n)} = -i(\phi^n/n!)(-1)^{(n-1)/2}M_0(x) \text{ for } n \text{ odd and } n \geqslant 1.$$

When $\Delta B \neq 0$, the perturbation series converge to equations (19).

3. Response functions of the system 'driven' by different basic excitations

The generalised imaging equation, (18), describes the NMR system's response to a single r.f. pulse. We shall briefly formulate the response functions for the different basic excitations discussed in § 1.4. The general principle to be noted here is that whereas the r.f. pulses affect the response $M(t)$ through the aperture function $F(\mathbf{r})$, the gradients modify the response through the phase term $\exp[i\gamma G(\mathbf{r})\cdot r]$. The ultimate image resolution is therefore affected by both functions, though primarily by the gradient. The response functions for the various excitations follow.

3.1 90° *and* 180° *broadband pulses*

This corresponds to $F(\mathbf{r})$ being a constant over the sample space. Geometrically, this implies that $B_1 \gg G_x L$, $t_p \ll T_2, T_1$ and $1/\gamma G_x L$, and $F(\mathbf{r}) = -i$, resulting in

$$m(t) = K \int_V \rho(\mathbf{r}) \exp(-i\pi/2) \exp[i\gamma G(\mathbf{r})\cdot \mathbf{r}t]\, \mathrm{d}V. \tag{23}$$

3.2 90° *and* 180° *narrowband pulses*

These pulses are primarily designed for 'slice' selection in the specimen being imaged. The condition here is $B_1 \cong G_x x$ for $x < L, t_p \ll T_1, T_2$ and $t_p \cong 1/\gamma G_x L$. For rectangular B_1-pulse, $F(x)$ has the form shown in (17).

3.3 *Readout gradient*

This is applied following a non-selective r.f. pulse, to effect the readout of the FID. The response function, or imaging equation, is

$$m(t) = \int_V \rho(\mathbf{r}) F(\mathbf{r}) L(\mathbf{r}) \exp[i\gamma G(\mathbf{r})\cdot \mathbf{r}t]\, \mathrm{d}V,$$

which is essentially a free evolution of the magnetisation in the absence of the r.f. excitation.

3.4 *Pulsed gradient*

The duration of the field gradient pulse is shorter than $1/\gamma G_x L$, so that the magnetisation is constant over the interval τ and

$$m(t) = K \int_V \rho(\mathbf{r}) \exp[i(\gamma G(\mathbf{r})\cdot r)\tau]\, \mathrm{d}V.$$

This is the key operative equation in Fourier zeugmatography (Kumar *et al* 1975).

4. Reception of the response signal: The NMR receiver

The magnetisation $m(t)$ described by (18), which is our system's response signal, is picked up by a coil. The induced e.m.f. is given by Faraday's law, expressed in the form

$$\varepsilon = -\frac{\partial}{\partial t}(\mathbf{B}_1 \cdot M_L(t)), \tag{24}$$

using the principle of reciprocity (Hoult and Richards 1976). Here $\mathbf{B}_1$ denotes the magnetic field produced by a unit current in the coil (assumed homogeneous over the specimen volume), and $M_L(t)$ is the magnetisation in the laboratory frame, related to $m(t)$ by

$$M_L(t) = m(t) \exp(i\omega_0 t),$$

and therefore the induced e.m.f., (24), is re-written as

$$\varepsilon = -iB_1 \omega_0 m(t) \exp(i\omega_0 t),$$

since the bandwidth of $m(t)$ is small compared with ω_0 (the 'narrowband' assumption). The coil is linearly polarised and the FID is given by

$$s(t) = B_1\omega_0 \operatorname{Re}[m(t)\exp(-i\pi/2)\exp(i\omega_0 t)]$$
$$= AB_1\omega_0 \operatorname{Re}\left[\left(\int_x M(x)\exp(i\gamma G_x x t)\,dx\right)\exp(-i\pi/2)\exp(i\omega_0 t)\right],$$

where $M(x) = F_{xy}(x)M_0(x)L(x,t)$ is in general complex,

$$M(x) = M_R(x) - iM_I(x).$$

Quadrature detection with reference signals $\cos\omega t$ and $\sin\omega t$, including low-pass filtering (LPF), gives

$$s_c(t) = \frac{AB_1\omega_0}{2}\operatorname{Re}\left[\int M(x)\exp(-i\pi/2)\exp[i(\omega_0+\gamma G_x x-\omega)t]\,dx\right],$$

and

$$s_s(t) = \frac{AB_1\omega_0}{2}\operatorname{Im}\left[\int M(x)\exp(-i\pi/2)\exp[i(\omega_0+\gamma G_x x-\omega)t]\,dx\right]. \quad (25)$$

Considering that in our experiments the detector reference ω is fixed, $(\omega_0 - \omega)\Delta\gamma G_x(L/2)$, it can be seen that $s(t)$ $(\Delta s_c(t) - is_s(t))$ may be Fourier-transformed to obtain $M(x)$. The phase introduced is in general different from $\pi/2$ due to the contribution from the receiver, and has to be corrected.

A special case of (25) arises when $F(x) = -i$, $L(x)$ is constant over x, and $\omega = \omega_0$. Here $s_c(t) = -\operatorname{Re}[\mathscr{F}^{-1}(M_0(x))]$, and $s_s(t) = -\operatorname{Im}[\mathscr{F}^{-1}(M_0(x))]$. This corresponds, of course, to a 1-D projection of the spin image $\rho(xyz)$.

The other situation encountered is $F(x) = F_x(x) - iF_y(y)$ and $L(x)$ constant over x. This represents a *selective pulse excitation*, where $F_{xy}(-(x+x_1)) = -F^*_{xy}(x+x_1)$, *i.e.*, case of a conjugate skew-symmetric aperture, while $M_0(x)$ is constant over $F(x+x_1)$. x_1 is related to ω (the operating frequency of the transceiver) by $\omega = \omega_0 + \gamma G_x x_1$.

In most modalities the signal is observed in the presence of a readout gradient, representing a combination of the two cases considered above.

4.1 *Noise considerations and spectrometer 'figure of merit'*

In addition to the FID, noise gets coupled to the system at various stages of the receiver, which degrades the quality of the spin image.

The source of noise is predominantly thermal, and may be assumed to be white Gaussian centred at the operating frequency. For the receiver bandwidth larger than the signal bandwidth (a condition pertinent to our spectrometer design), the noise is assumed to be a bandpass, white Gaussian process. Defining $n_c(t)$ and $n_s(t)$ as the quadrature noise components, $K_{sc}(\tau)$ (the cross-correlation) is zero, as the spectrum of $n(t)$ is symmetric about the carrier. For a real function $M_0(\omega(x))$, $\mathscr{F}^{-1}(S_c(t) - is_s(t))$ is real; and the reconstructed image is $M_0(\omega) + N(\omega)$, where $N(\omega) = \operatorname{Re}(N_c(\omega))$ $+ \operatorname{Im}(N_s(\omega))$. In general, where $M_0(\omega)$ is complex, the image may be defined as $M_0(\omega)$ and the noise will be a Rayleigh-distributed random variable for any ω.

The signal-to-noise ratio (S/N), or 'figure-of-merit', may now be evaluated for the bandpass signal $f(t)$ (*i.e.*, the signal is assumed to be time-limited by observation). For

$M(x) = M_0$, a constant,

$$f(t) = \omega_0 B_1 A \operatorname{Re}\left\{\int_{-L/2}^{L/2} [\exp(i\gamma G_x x t)\,dx]\exp(i\omega_0 t)\right\}$$

$$= \omega_0 B_1 AL \left(\frac{\sin\gamma\frac{G_x L}{2}t}{\gamma\frac{G_x L}{2}t}\right)\cos\omega_0 t. \tag{26}$$

The signal is gated 'on' from $t = 0$ (or actually t_p, which is *small* compared with $1/\gamma G_x L$ and T_2). The energy, E_s, in the signal envelope is given by

$$E_s = \int_{-\infty}^{\infty} \omega_0^2 B_1^2 V^2 \frac{\sin^2\gamma\frac{G_x L}{2}t}{\left(\gamma\frac{G_x L}{2}t\right)^2}\,dt$$

$$= \omega_0^2 B_1^2 V^2 \pi T_2^*, \left(T_2^* \sim \frac{1}{\gamma G_x L} \text{ for strong gradients}\right). \tag{27}$$

From (27), the maximum S/N obtainable is

$$E_s/N_0 = \omega_0^2 B_1^2 V^2 \pi T_2^*/N_0, \tag{28}$$

where N_0 is the white noise power spectral density (if the signal is known *a priori*). This ratio, then, is used as a representative figure-of-merit, as it is based on the assumption that $M(x) = M_0$. Though the spin density variation, $\rho(\mathbf{r})$, and the relaxation time variations $T_1(\mathbf{r})$ and $T_2(\mathbf{r})$ carry the imaging information (as contrast), these variations are usually small in a sample and hence the bulk sensitivity of the system is indicated by (28), which compares well with the E_s/N_0 derived earlier for a pulsed NMR experiment (Ernst and Anderson 1966).

The overall system identification in terms of system-input and system-response is depicted in figure 5.

5. Spectrometer design considerations

This section considers various aspects of design strategy we have adopted in configuring a 15 MHz proton imaging spectrometer for studying multiphase bio-samples. The block schematic of the system, shown in figure 6, is broadly categorised into (i) the r.f. probe (ii) the r.f. pulsed power transmitter and receiver (transceiver), (iii) magnetic field and magnetic field gradient control, and (iv) signal acquisition and averaging.

5.1 *The sample coupling r.f probe*

This is the 'heart' of the system, acting as an interface between the specimen under study and the transmitted and received electrical signals. It consists of a tuned r.f. coil. A single coil geometry is employed, usually of a solenoidal or 'saddle' shape, though single turn

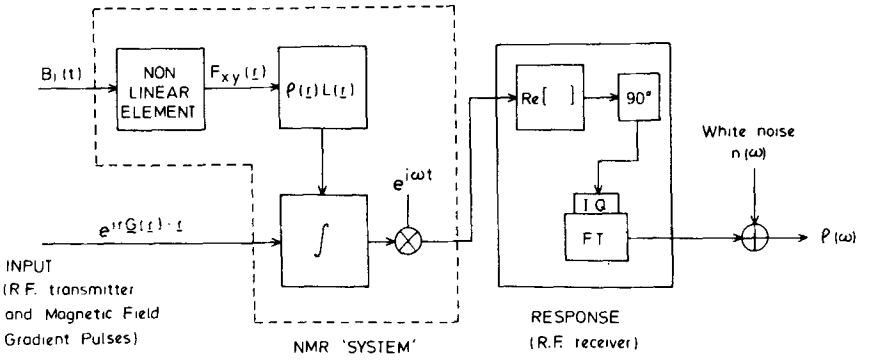

Figure 5. Overall system identification in terms of input (r.f. transmitter pulse and the magnetic field gradient) and response (magnetisation) as seen by the r.f. receiver. In the receiver section, Re[ ] denotes the real, or in-phase, signal response component, and IQ denotes the imaginary, or quadrature, response component. $n(\omega)$ denotes white noise at the output.

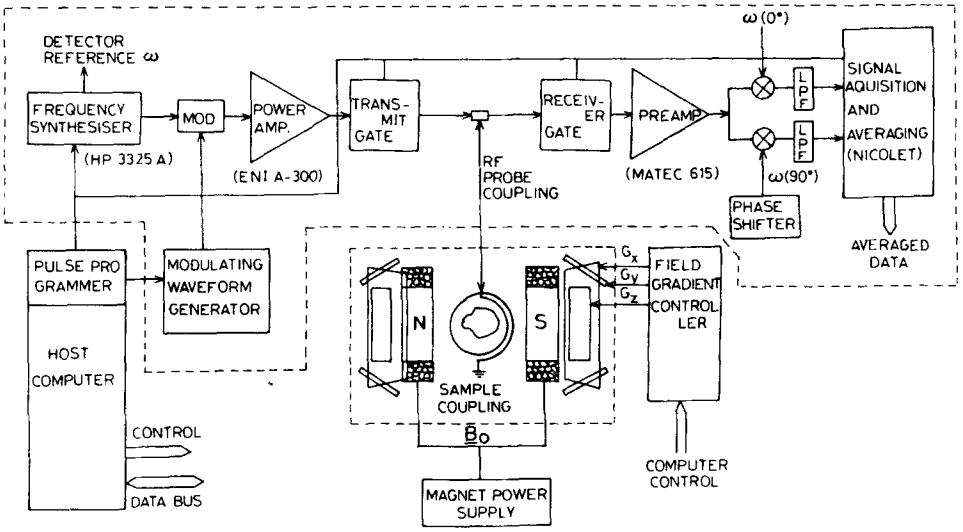

Figure 6. Block schematic of our NMR imaging spectrometer. The dotted section corresponds to the overall 'system' identified earlier.

loop 'pairs' are known to be used in 'crossed coil' arrangements. As the solenoidal and saddle-shaped coils produce linearly polarised $\mathbf{B}_1$ fields, only half the current is effective for sample excitation.

The performance of the coil is measured in terms of r.f. field uniformity and coupling efficiency (related to S/N). As these requirements conflict, a trade-off is employed. For example, the solenoid configuration has a 10 dB S/N advantage over a saddle-shape of the same dimensions, though the field uniformity is poorer. For a 'solenoid *vs* saddle-shape' radius ratio of ~ 2, the S/N advantage is still ~ 7 dB in favour of the solenoid. The effective volume inside the coil is 5×10^{-5} m^3, which is nearly an order of magnitude larger than the sample volumes intended in our studies, thereby ensuring good B_1 homogeneity over the sample.

5.2 *The r.f. transceiver*

Here the essential features of the transmitter section are (a) generation of pulsed r.f. from a programmer unit based on an 8253 on-board counter chip of a commercial microprocessor (VMC-85); pulse timing sequences (see Dick 1976; Adduci and Gerstein 1979) are derived from this chip, (b) high pulsed power from the transmitter amplifier, (c) impedance matching with the 'load' (which is the sample coil resonant circuit), (d) small post-transmit 'deringing' time τ_d, (e) a short rise-time (or large bandwidth) power amplifier, (f) modulating signals for selective pulse excitations, and (g) a 'transmit' switch offering low 'on' attenuation and high 'off' isolation, to decouple transmitter noise from the sample coil during reception of FID.

In the receiver section, the following are incorporated: (a) a low noise-figure preamplifier, (b) efficient noise and signal power matching of the source (the sample coil) with the receiver preamplifier, (c) quadrature demodulator/detector for recovering the baseband signal (with an anti-aliasing filter), and (d) r.f. switches with high isolation to protect the receiver from high-power r.f. pulses and low 'on' attenuation, and shot-noise contribution, during signal reception.

The specifications for an ENI A-300 broadband power amplifier and a 'Matec' r.f. preamplifier-receiver have been assumed in our design of the transceiver circuit. In table 1 are listed the parameters for the system we have developed. The deringing time, τ_d, is estimated for the worst-case values of T_2^* ($\sim 1/\gamma G_x L$) and T_2. The resistance (R), inductance ($\mathscr{L}$), quality factor (Q_c max.) and the distributed capacitance (C_d) of the solenoidal coil used in our work are given along with peak (I_p) and average (I_{av}) current and the B_1 requirements for $t_p \sim 5\ \mu$s and $\phi = 90°$.

5.3 *Magnetic field and gradient control*

For a proton resonance frequency of $\sim$ 15 MHz the B_0 field falls in the 0·3T* range, and this is supplied by a research electromagnet whose central field has been shimmed

Table 1. NMR imaging spectrometer: Important design parameters.

Parameter	Value
T_2^* (for 5 μT cm^{-1})	$2{\cdot}27 \times 10^{-4}$ s
T_2	50 μs–5 ms
T_1	5 ms–500 ms
τ_d	$\leqslant (50 \times 10^6/100) \cong 0{\cdot}5\ \mu$s
$R^{(a)}$	0·011 n^2 ohms
$\mathscr{L}$	0·027 n^2 μH
Q_c (max)	200
C_d	10 pf
I_p	106/n amp.
I_{av}	$(1/\sqrt{2})(106/n)$ amp.
$B_1^{(b)}$	$2{\cdot}22 \times 10^{-5}$ nT

(a) n = Number of turns of probe coil.
(b) B_1 is calculated for $\phi = 90°$, $t_p = 5\ \mu$s.

*$T \equiv 1$ Tesla $= 10^4$ gauss.

to about 10 parts per million homogeneity with ferromagnetic plating and electrical compensation coils.

For the gradient coil system, three pairs of coils are used for the x, y and z directions. The x and y gradient coils are of saddle-shaped geometry, as this is known to give acceptable higher-order spatial field nonlinearity. In the z-direction, we employ a Helmholtz pair mounted on the magnet pole-faces. These three sets of coils are energised by a microprocessor-controlled current driver built from a low-drift operational amplifier (LM 308). Typical gradients of 10–50 μT cm^{-1} (with $\sim 1\%$ linearity over the sample volume) are achievable, enabling an upper limit image resolution of 1 mm (corresponding to a frequency resolution of 200 Hz). The ampere-turns (AT) required for 50 μT cm^{-1} gradient is 12 AT for Helmholtz pair with a diameter-to-length ratio (D/l) = 1 and 19 AT for D/l = 0·5. Since the latter ratio is optimum in the sense that the second and third field derivatives at the centre of the coil are equal to zero, we have preferred 19 AT in our design.

The theoretical S/N (equation (28)) is $E_s/N_0 = 70$ dB for $T_2 = 2{\cdot}27 \times 10^{-4}$ s and 55 dB for $T_2 = 50$ μs for whole-sample excitations. This corresponds to the FID from a single image projection. A set of six to eight projections in a plane are tractable for reconstruction of the image, considering the software complexity. The resulting E_s/N_0 is 77 dB (taking into account signal averaging). The corresponding (0 dB S/N) resolution is $\Delta V = 5{\cdot}32 \times 10^{-10}$ m^3 (or $\Delta x = 1$ mm). Our instrumentation is limited to off-line projection reconstruction as the operational modality.

5.4 *Signal acquisition and sampling*

The FID after demodulation is recorded digitally. The minimum sampling rate F_s is determined by the Nyquist criterion, $F_s > 2 \times$ [signal bandwidth] where the bandwidth may be given by $2 \times 10 \times (1/2\pi T_2)$, while the number of 'samplings' per unit bandwidth is determined by resolution considerations. The intrinsic resolution is considered to be $(1/t_w)$ where t_w is the acquisition-time window. The FID corresponding to our simple case of 1-D projection is written as $V_s = V_0$ since $(\gamma G_x L t/2\pi)$. Calculation of the time at which V_s would roughly fall to the rms noise voltage should yield a lower limit to the observation time.

In our spectrometer system, a 'Nicolet 1174' high speed (1 μs per point per input) signal digitizer/averager with an 8-bit analogue-to-digital resolution is used, which acquires and stores the time-averaged information on the point-by-point FID data samplings. The 1174 memory stores 4K × 20 bits of digitised signal. The stored data are transferred to a DEC 1090 computer for off-line image processing.

6. Conclusions

We have discussed NMR imaging from the viewpoint of system design. Models based on Bloch equations and rotating frame formalism provide a useful mathematical description of different NMR imaging schemes. The response, namely, the magnetisation $M_{xy}(t)$, is linearly related to the system identification function $\rho(\mathbf{r})L(\mathbf{r}, t)$ while the r.f. excitation affects the system nonlinearly and appears as an 'aperture' function in the imaging equation. Solution of the imaging equation for a rectangular r.f. pulse is possible in closed form, while for other pulses it is obtained numerically. In selective excitation modalities, the choice of pulses for signal design can be made by

approximating the system by the linear term $M_{xy}^{(1)}(t)$ in a perturbation expansion.

Spectrometer design considerations indicate that the resolution is limited by noise at the detection stage, and that the solenoidal r.f. probe configuration has a significant S/N advantage over the saddle-shaped configuration, although the r.f. field homogeneity is better in the latter. In the case of our NMR imaging spectrometer developed for studying multiphase biospecimens, a 1 mm image resolution is feasible with a gradient of 50 μT cm^{-1}, assuming a 200 Hz frequency resolution and signal averaging.

Acknowledgement

Thanks are due to the Department of Science and Technology (DST), Government of India, for supporting this work in the form of a research grant to one of the authors (PR).

References

Abragam A 1961 *The principles of nuclear magnetism* (London: Oxford University Press)
Adduci D J and Gerstein B C 1979 *Rev. Sci. Instrum.* **50** 1403
Bloch F 1946 *Phys. Rev.* **70** 460
Caprihan A 1983 *IEEE Trans. Medical Imaging* **MI-2** 169
Carr H Y and Purcell E M 1954 *Phys. Rev.* **94** 630
Cho Z H, Kim H S, Song H B and Cumming J 1982 *Proc. IEEE* **70** 1152
Dick I R 1976 *J. Phys.* **E9** 1054
Ernst R and Anderson W A 1966 *Rev. Sci. Instr.* **37** 93
Hahn E L 1950 *Phys. Rev.* **80** 580
Hinshaw W S 1976 *J. Appl. Phys.* **47** 3709
Hinshaw W S and Lent A H 1983 *Proc. IEEE* **71** 338
Hoult D I 1979 *J. Mag. Res.* **35** 69
Hoult D I and Richards R E 1976 *J. Mag. Res.* **24** 71
Hounsfield G, Ambrose J and Perry J 1973 *Br. J. Radiol.* **46** 1016
Kumar A, Welti D and Ernst R 1975 *J. Mag. Res.* **18** 69
Lauterbur P C 1973 *Nature (London)* **242** 190
Locher P R 1984 *Philips Tech. Rev.* **41** 73
Mansfield P and Maudsley A 1976 *J. Phys.* **E9** 271
Mansfield P, Maudsley A A, Morris P G and Pykett I L 1979 *J. Mag. Res.* **33** 261
Maudsley A A 1980 *J. Mag. Res.* **41** 112
Raghunathan P 1981 *Proc. Indian Acad. Sci. (Chem. Sci.)* **90** 467
Scudder H J 1978 *Proc. IEEE* **66** 628